A sensitivity study of climate and energy balance simulations with use of satellite-derived emissivity data over Northern Africa and the Arabian Peninsula

L. Zhou,[1] R. E. Dickinson,[1] Y. Tian,[1] M. Jin,[2] K. Ogawa,[3] H. Yu,[1] and T. Schmugge[3]

Received 18 August 2003; revised 19 September 2003; accepted 10 October 2003; published 27 December 2003.

[1] This paper analyzes the sensitivity of simulated climate and energy balance to changes in soil emissivity over Northern Africa and the Arabian Peninsula and considers how this information may be used to improve emissivity parameterizations in climate models. Analysis of satellite observations suggests that the soil emissivity in current models is too high over this region. Sensitivity tests based on the recently developed Community Land Model indicate that this bias could produce significant errors in the model simulated ground and air temperature, net and upward longwave radiation, and sensible heat flux. There is a linear relationship between changes in emissivity and changes in these variables. Statistical results show that, on average for the study region, a decrease of soil emissivity by 0.1 will increase ground and air temperature by about 1.1°C and 0.8°C and decrease net and upward longwave radiation by about 6.6 Wm^{-2} and 8.1 Wm^{-2}, respectively, at the ground surface. The decreased net longwave radiation (less emission) is mainly balanced by an increase of sensible heat flux of about 5.9 Wm^{-2}. These relations vary seasonally and diurnally. The temperature increases are slightly higher in winter than in summer and twice as large during nighttime as during daytime, while the sensible heat flux and longwave radiation show more change in summer/daytime than in winter/nighttime. Our experimental results are consistent with our theoretical energy balance analyses. When a more realistic emissivity value is used, the model cold bias over the Sahara in comparison with land surface air temperature observations could be partially reduced. These results indicate that the simple representations of the land surface emissivity in climate models, especially for bare soil, need improvements based on satellite and in situ observations. *INDEX TERMS:* 1620 Global Change: Climate dynamics (3309); 1640 Global Change: Remote sensing; 3322 Meteorology and Atmospheric Dynamics: Land/atmosphere interactions; 3337 Meteorology and Atmospheric Dynamics: Numerical modeling and data assimilation; *KEYWORDS:* emissivity, climate model, MODIS, ASTER

Citation: Zhou, L., R. E. Dickinson, Y. Tian, M. Jin, K. Ogawa, H. Yu, and T. Schmugge, A sensitivity study of climate and energy balance simulations with use of satellite-derived emissivity data over Northern Africa and the Arabian Peninsula, *J. Geophys. Res.*, *108*(D24), 4795, doi:10.1029/2003JD004083, 2003.

1. Introduction

[2] Emissivity is defined as the ratio of thermal radiation emitted by a surface to that of a blackbody. As an important parameter required in climate models, it determines how much thermal radiation is emitted back to the atmosphere and space and therefore the surface radiation budget. Consequently, it determines important climate variables such as temperature [*Dickinson et al.*, 1993; *Bonan*, 1996; *Sellers et al.*, 1997].

[3] Emissivity changes as surfaces change, depending not only on the chemical composition, texture and structure of the underlying soil, but also on the amount of vegetation cover and soil moisture [*Prabhakara and Dalu*, 1976; *Salisbury and D'Aria*, 1992; *Wilber et al.*, 1999; *Ogawa et al.*, 2002, 2003]. Current climate models represent the land surface emissivity by either a constant value or very simple parameterizations due to very limited observations. For example, the land surface emissivity is prescribed to be unity in GCMs of the Center for Ocean-Land-Atmosphere Studies (COLA) [*Kinter et al.*, 1988], the Chinese Institute of Atmospheric Physics (IAP) [*Zeng et al.*, 1989], and the US National Meteorological Center (NMC) Medium-Range Forecast (MRF) [*NMC Development Division*, 1988] and a constant soil emissivity of 0.96 is used in the recently developed Common Land Model (CLM0) [*Zeng et al.*, 2002; *Dai et al.*, 2003] and Community Land Model (CLM2) [*Bonan et al.*, 2002]. Such simple repre-

[1]School of Earth and Atmospheric Sciences, Georgia Institute of Technology, Atlanta, Georgia, USA.
[2]Meteorology Department, University of Maryland, College Park, Maryland, USA.
[3]USDA/ARS Hydrology and Remote Sensing Lab., Beltsville, Maryland, USA.

0148-0227/03/2003JD004083$09.00

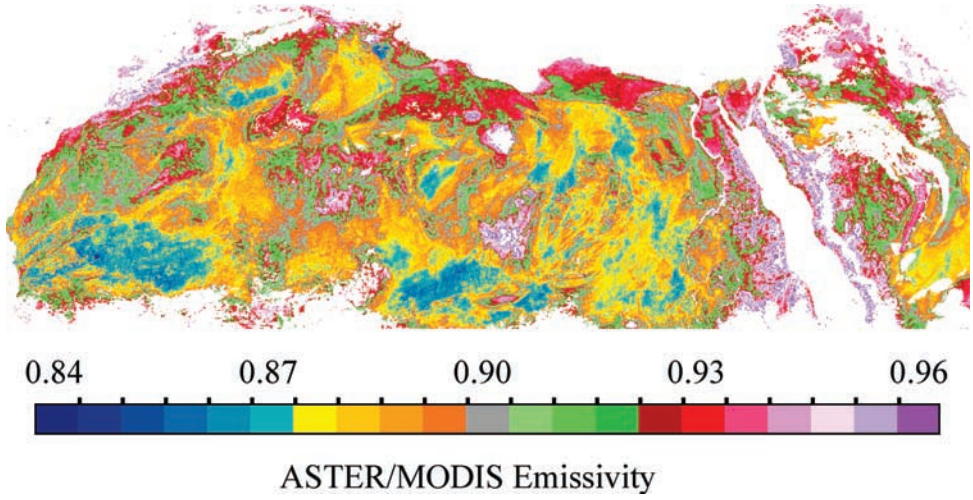

Figure 1. Spatial distributions of emissivity (8–13.5 μm) over the Sahara desert and Arabian Peninsula at 0.05° resolution [*Ogawa et al.*, 2004].

sentations neglect the spatial and spectral variations of emissivity.

[4] Satellites provide information with global spatial sampling at regular temporal intervals and thus have the capability to estimate accurately model parameters globally. Unlike what has been included in climate models up to now, satellite observations from the Advanced Spaceborne Thermal Emission and Reflection Radiometer (ASTER) and MODerate Resolution Imaging Spectroradiometer (MODIS) show significant spatial variability of surface emissivity over deserts and semi-deserts [*Ogawa et al.*, 2002, 2003; *Jin and Liang*, 2004; *Zhou et al.*, 2003a]. In particular, the window (8–12 μm) emissivity for bare soil over the northern Sahara desert ranges from 0.81 to 0.95 [*Ogawa et al.*, 2003]. Such variability suggests that climate models may need to better represent the land surface emissivity based on satellite observations.

[5] Can a model's unrealistic treatment affect regional surface climate and energy balance? Would a more realistic emissivity representation improve climate simulations in current climate models? For example, the CLM2 demonstrates a cold bias of several degrees in the Sahara throughout the year [*Bonan et al.*, 2002]. Possibly, this is in part due to the error or inaccurate specification of land surface properties in the model. Among the model parameters, vegetation related variables could not be responsible for such a cold bias since there is little vegetation over this region. The model values of albedo and emissivity can be very different from those determined from satellite observations [*Oleson et al.*, 2003; *Zhou et al.*, 2003a, 2003b] and so use of satellite data may improve the modeled temperature. Use of MODIS albedo, however, makes the cold bias worse since MODIS gives higher albedos than used in the model. So, could the errors in emissivity contribute to the cold bias?

[6] To clarify this question, we perform a sensitivity study with more realistic emissivity values from MODIS and ASTER to test the sensitivity of simulated climates and energy balance to changes in soil emissivity over Northern Africa and the Arabian Peninsula. We focus on this region not only because the largest emissivity bias was observed

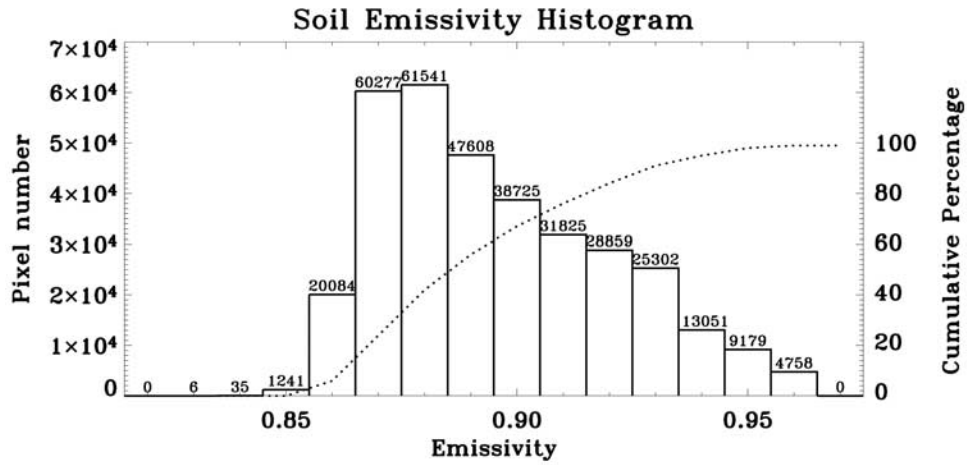

Figure 2. Histograms of emissivity over non-vegetated pixels in Figure 1, defined as those grid cells that contain only non-vegetated 1 km subpixels according to the MODIS land cover map [*Friedl et al.*, 2002].

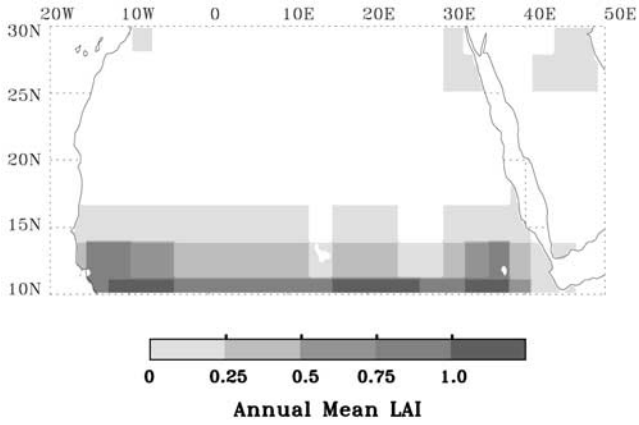

Figure 3. Study region in the Sahara desert and Arabian Peninsula (10°N–30°N, 20°W–50°E), together with the annual average leaf area index (LAI) used in the CLM2.

there [*Ogawa et al.*, 2002, 2003; *Zhou et al.*, 2003b] but also because the near absence of vegetation could make this issue less complex. As the first step, this paper considers how this information may be used to improve emissivity parameterizations in climate models. Section 2 describes the land surface model used in this study and designed sensitivity experiments based on satellite observations. Section 3 analyzes relationships between changes in soil emissivity and changes in simulated climate and energy balance. Section 4 concludes the major results.

2. Data and Design of the Experiments

2.1. Satellite Derived Emissivity

[7] Before designing the sensitivity experiments, we need to determine from satellite observations reasonable values for surface emissivity. An important question is whether satellite derived emissivities in the window region (8–12 μm) or in an even broader spectral band (e.g., 3–100 μm) should be used? *Ogawa et al.* [2004] provide a detailed discussion of this issue. They compared the net longwave radiation integrated over several wide wavelength ranges for 314 emissivity spectral samples and several land surface temperatures under a US standard atmosphere profile. They found that the emissivity between 8 and 13.5 μm is best for climate models that require surface emissivity for calculation of net longwave radiation since a large part of the net longwave radiation is located in 8–13.5 μm under cloud free condition.

[8] We use the 8–13.5 μm emissivity data generated by linear regressions between ASTER emissivity and MODIS reflectance and emissivity data [*Ogawa et al.*, 2004] to provide the continental coverage not available from ASTER because of its small coverage (60 km swath). ASTER has five spectral channels (8.125–8.475, 8.475–8.825, 8.925–9.275, 10.25–10.95, 10.95–11.65 μm) in the window region and thus may give a more reliable spectral to broadband emissivity conversion than MODIS, which has only one channel in 8–9.5 μm where the largest range of emissivity is observed. The linear regression was calibrated using the MODIS products (MOD43 for reflectance and MOD11B1 for emissivity) and the emissivity map derived from the ASTER five channel emissivities at 90 m resolution for a 520 × 1400 km^2 area over Algeria, Libya, and Tunisia in North Africa [*Ogawa et al.*, 2003]. The regression was validated using MODIS products and the ASTER emissivity data over an area of about 400,000 km^2 in North Africa and the Arabian peninsula outside of the previous calibration area. The expected error of emissivity is about 0.02 [*Ogawa et al.*, 2004]. A USGS 1 km resolution land cover map was used to remove vegetated pixels. Details about this data set and its validation are described in *Ogawa et al.* [2004].

[9] Figure 1 shows spatial distributions of emissivity over the Sahara desert and Arabian Peninsula at 0.05° resolution. Evidently, the majority of pixels show an emissivity value less than 0.96, the value used for soil in the CLM0 and CLM2. Pixels with the lowest emissivities in blue are pixels where sands, rock, and barren land (referred as bare soil) are located, while pixels with the highest values in red and pink are partially vegetated. Since vegetation is heterogeneous and varies seasonally in deserts and semideserts and the emissivity of bare soil is our major concern, we use the MODIS land cover map [*Friedl et al.*, 2002] at 1 km resolution to further remove those partially vegetated 0.05° pixels. We adopt the purity concept of *Tian et al.* [2002] to retain only the non-vegetated pixels with a purity of 100%, i.e., each of these 0.05° pixels contains only non-vegetated 1 km subpixels according to the MODIS land cover map. Figure 2 shows the histogram over these non-vegetated pixels. The bare soil emissivity ranges from 0.83 to 0.96, with most values between 0.87 and 0.92. Of the total 342491 pixels, 76% have values less than 0.92 and 24% less than 0.88.

2.2. Design of the Experiments

[10] Here we use the documented CLM2 version of *Bonan et al.* [2002]. CLM2 is a one-dimension land surface parameterization of energy, momentum, water and CO_2 exchange between the atmosphere and land. It is largely based on CLM0 [*Zeng et al.*, 2002; *Dai et al.*, 2003] but has retained some features of the NCAR Land Surface Model [*Bonan*, 1996]. The emissivity in the CLM2 is set as 0.97 for snow, lake, and glaciers, and 0.96 for soil and wetlands. The vegetation emissivity is defined as, $1 - \exp(-LSAI)$, where *LSAI* represents stem and leaf area index. The net longwave radiation flux over the land surface in CLM2 is calculated as a sum of fluxes for vegetation and its underlying ground. For non-vegetated surfaces ($LSAI = 0$), the flux is only from the ground.

[11] Figure 3 shows our study region in the Sahara desert and Arabian Peninsula (10°N–30°N, 20°W–50°E), together with the annual average leaf area index used in the CLM2. Simulations over this region have been commonly examined [e.g., *Bonan*, 1996; *Bonan et al.*, 2002; *Zeng et al.*, 2002]. Since the satellite derived emissivity of bare soil ranges from 0.83 to 0.96 (Figure 2), we design four experiments by replacing the model soil emissivity of 0.96 in our study region by 0.92, 0.90, 0.88, and 0.84, respectively, and one control run to test the sensitivity of climate and energy balances. In total, five 20-year simulations are executed from CLM2 coupled with Community Atmosphere Model (CAM2) with resolution at about 2.8° x 2.8° using observed sea surface temperature and sea ice from January 1979 to December 1998. Besides standard model outputs, we also print out hourly outputs for 2m height air temperature, net and upward longwave radiation, and sensible heat flux for diurnal cycle analysis.

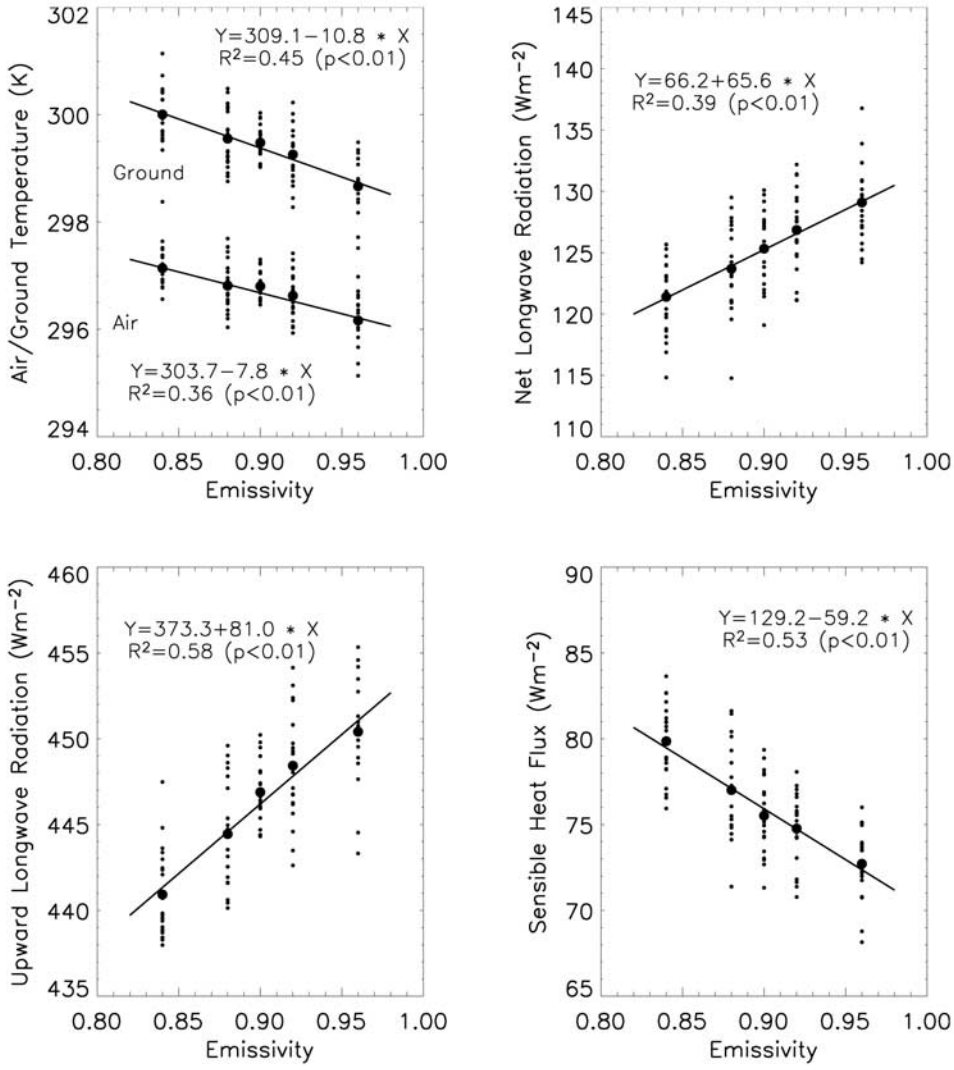

Figure 4. Changes in annual mean ground and air temperature, net longwave radiation, upward longwave radiation, and sensible heat flux as a function of the soil emissivity of 0.96, 0.92, 0.90, 0.88, and 0.84. The smaller dot represents annual means and the larger dot represents the 20-year average. A linear regression was fit to each variable for the annual means, with a total of 100 samples (20 years × 5 simulations), and its slope is estimated to assess how much the variable will change for a unit change of emissivity. The significance of each regression is also shown.

[12] Figure 3 also shows the presence of vegetation in the southern boundary of the Sahara desert. Since we focus our study on bare soil only, both spatial distributions and regional averages of model outputs are analyzed mainly over non-vegetated grid cells. The regional averages are performed over a smaller area (17°N–30°N, 0°E–30°E), located in the center of our study region, to reduce possible impacts from vegetation and surrounding water. Averaging over this small region also allows diurnal cycles of model variables to be composited with the model universal time (UT) calculation.

3. Results

3.1. Theoretical analysis

[13] Over non-vegetated surfaces, the net longwave radiation flux, $\bar{L}$ (Wm^{-2}), the sensible heat flux, H (Wm^{-2}), the latent heat flux, λE (Wm^{-2}), and the soil heat flux, G (Wm^{-2}) depend on the ground temperature, T_g (K). The surface fluxes and temperature in CLM2 are calculated by finding T_g that balances the energy budget,

$$-S + \bar{L}(T_g) + H(T_g) + \lambda E(T_g) + G(T_g) = 0, \qquad (1)$$

where S is the net solar radiation (Wm^{-2}) at the ground surface. $\bar{L}$, H, λE are defined as positive toward the atmosphere, and G is defined as positive toward the soil. The $\bar{L}$ is given by,

$$\bar{L} = L\uparrow - L\downarrow = -\alpha_g L\downarrow + \varepsilon_g \sigma T_g^4, \qquad (2)$$

where σ is the Stefan-Boltzmann constant ($\sigma = 5.67 \times 10^{-8}$ $\mathrm{Wm}^{-2}\mathrm{K}^{-4}$), α_g and ε_g stand for the ground absorptivity and emissivity, respectively, $L\downarrow$ stands for the

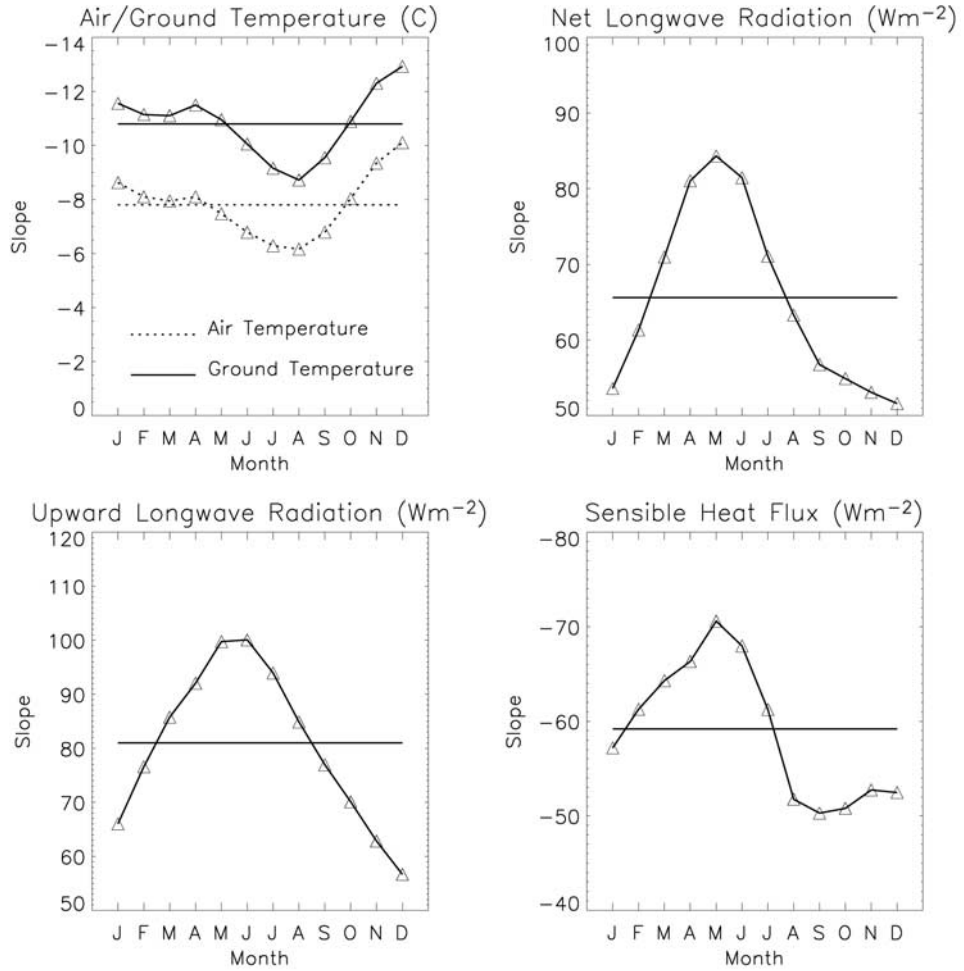

Figure 5. Seasonal variations of the estimated slopes for ground and air temperature, net longwave radiation, upward longwave radiation, and sensible heat flux. The slopes are estimated as Figure 4. The constant lines represent the slopes of Figure 4. The symbol "Δ" denotes the slopes that are statistically significant at the 5% level.

downward atmospheric longwave radiation, and $L\uparrow$ stands for the upward longwave radiation, defined as,

$$L\uparrow = (1-\alpha_g)L\downarrow + \varepsilon_g \sigma T_g^4. \tag{3}$$

We assume that the spectral distribution of downward sky radiation is close enough to that of blackbody. This allows us to assume α_g to be equal to ε_g. Equation (2) becomes

$$\bar{L} = \varepsilon_g(\sigma T_g^4 - L\downarrow), \tag{4}$$

[14] A change of emissivity can be compensated for by a change in T_g to produce the same emission. However, the implied changes of T_g will generally in turn change sensible and latent fluxes as well as soil heat fluxes. These fluxes may modify cloud properties and thus solar radiation. For an arid region, the annual average change in longwave radiation should be largely balanced by that in sensible heat flux. The actual T_g must continue to maintain energy balance. Therefore, with a change in ε_g, the new balance from equation (1) will be,

$$\Delta\bar{L}(T_g) + \Delta H(T_g) \approx 0, \tag{5}$$

where Δ preceding any of the terms denotes a small change in that variable due to a change in emissivity ($\Delta\varepsilon_g$). This equation suggests that less longwave emission ($\Delta\bar{L} < 0$) at the ground will be balanced by increased sensible heat flux ($\Delta H > 0$) or vice versa.

[15] If $L\downarrow$ remains constant, for a given $\Delta\varepsilon_g$, the ΔT_g versus $\Delta\bar{L}$ relation can be derived from equation (4) by,

$$\frac{\Delta T_g}{\Delta\varepsilon_g} = \frac{1}{4\sigma\varepsilon_g T_g^3}\left[\frac{\Delta\bar{L}}{\Delta\varepsilon_g} - (\sigma T_g^4 - L\downarrow)\right]. \tag{6}$$

Apparently, this is a linear relationship. Our simulation results in the next section indicate that both ($\Delta\bar{L}/\Delta\varepsilon_g$) and ($\sigma T_g^4 - L\downarrow$) are positive and the latter is always larger than the former, i.e., ($\Delta T_g/\Delta\varepsilon_g$) < 0. This means that a decrease in ground emissivity ($\Delta\varepsilon_g < 0$) will always result in increases of both ground temperature ($\Delta T_g > 0$) and sensible heat flux ($\Delta H > 0$) and a decrease in the net longwave radiation ($\Delta\bar{L} < 0$) due to the decrease in the upward longwave radiation ($\Delta L\uparrow < 0$). The magnitude of

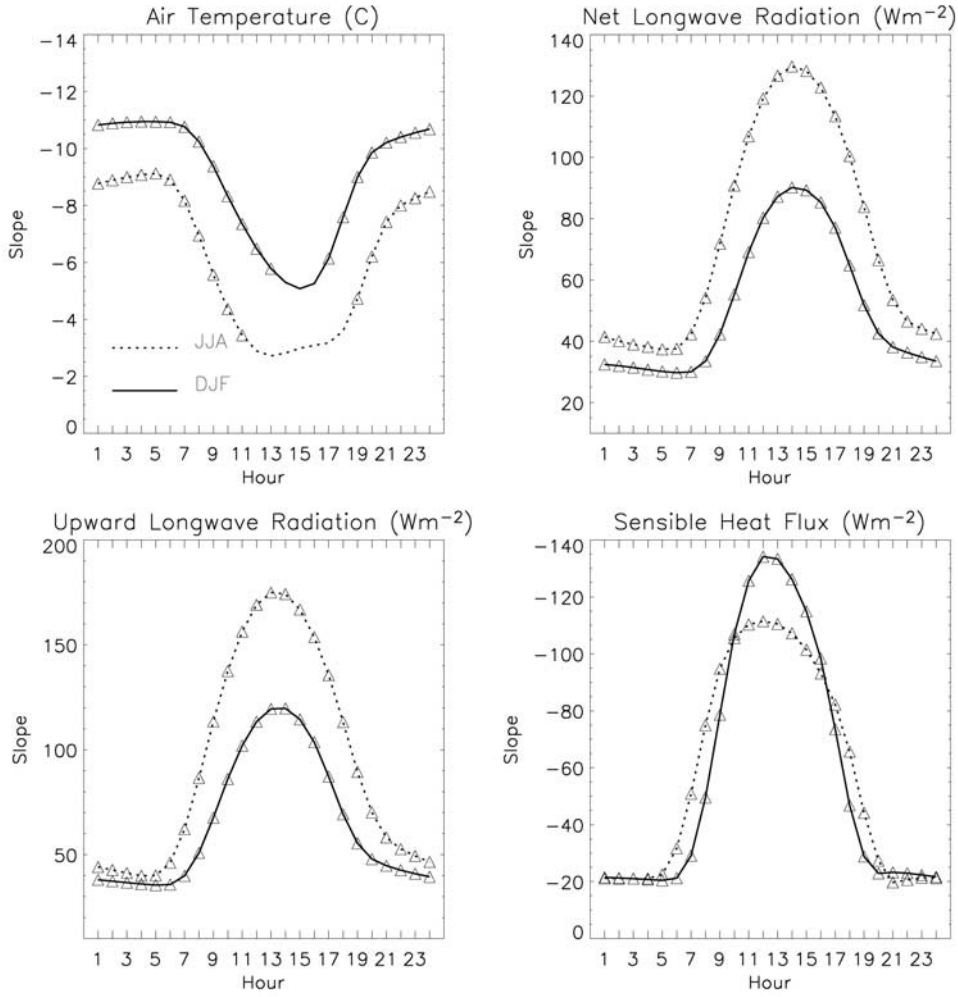

Figure 6. Diurnal variations in universal time of the estimated slopes for air temperature, net longwave radiation, upward longwave radiation, and sensible heat flux in winter (DJF) and summer (JJA). The slopes are estimated as Figure 4. The symbol "Δ" denotes the slopes that are statistically significant at the 5% level.

these changes is proportional to that of the emissivity change.

3.2. Simulated Climates and Energy Balance

[16] Significant changes are found for 2 m height (air) temperature (T_a), ground temperature (T_g), net longwave radiation ($\bar{L}$), upward longwave radiation ($L\uparrow$) and sensible heat flux (H) over the region where the ground emissivity (ε_g) is altered.

[17] Figure 4 shows how regional averaged annual means of T_g, T_a, $\bar{L}$ $L\uparrow$, and H vary as ε_g decreases from 0.96 to 0.84. A linear regression is fit to each variable and its slope is estimated to assess how much the variable will change for a unit change of emissivity. Evidently, T_a, T_g, and H increase linearly as a result of decreased $\bar{L}$ (less emission) and $L\uparrow$, and all slopes are statistically significant at the 1% level. Regression results indicate that a soil emissivity lower by 0.1 will cause (a) ground temperature higher by 1.1°C, (b) air temperature higher by 0.8°C, (c) net longwave radiation lower by 6.6 Wm^{-2}, (d) upward longwave radiation lower by 8.1 Wm^{-2}. The decreased longwave emission at the ground, 6.6 Wm^{-2}, is mainly balanced by increased sensible heat flux, 5.9 Wm^{-2}, to the atmosphere. These results are consistent with the theoretical analysis in section 3.1. For example, when the regional averaged annual means of T_g (298.7°K), $L\downarrow$ (321.2 Wm^{-2}), ε_g (0.96), and $\Delta\bar{L}/\Delta\varepsilon_g$ (65.6 Wm^{-2}) are put into equation (6), we get $(\Delta T_g/\Delta\varepsilon_g) = -11.0$°C, comparable with the slope of −10.8°C estimated from the regression. Some interannual variations are observed due to variations and feedbacks of T_g and $L\downarrow$ in equation (6) and changes of other terms in equation (1).

[18] The above relations should vary seasonally and diurnally with changes of $\bar{L}$ and T_g in equation (6). To assess such variations, we fit linear regressions for regional averaged monthly and hourly means of T_a, T_g, $\bar{L}$, $L\uparrow$, and H, and estimate their slopes as done in Figure 4. Figure 5 shows the seasonal variations of the estimated slopes. Evidently, T_a and T_g increase about 2°C more in winter than in summer for a unit decrease of emissivity. This seasonal difference can be explained by that of $\bar{L}$ in equation (6), which shows the largest slope in summer, i.e., a larger $(\Delta\bar{L}/\Delta\varepsilon_g)$ will result in

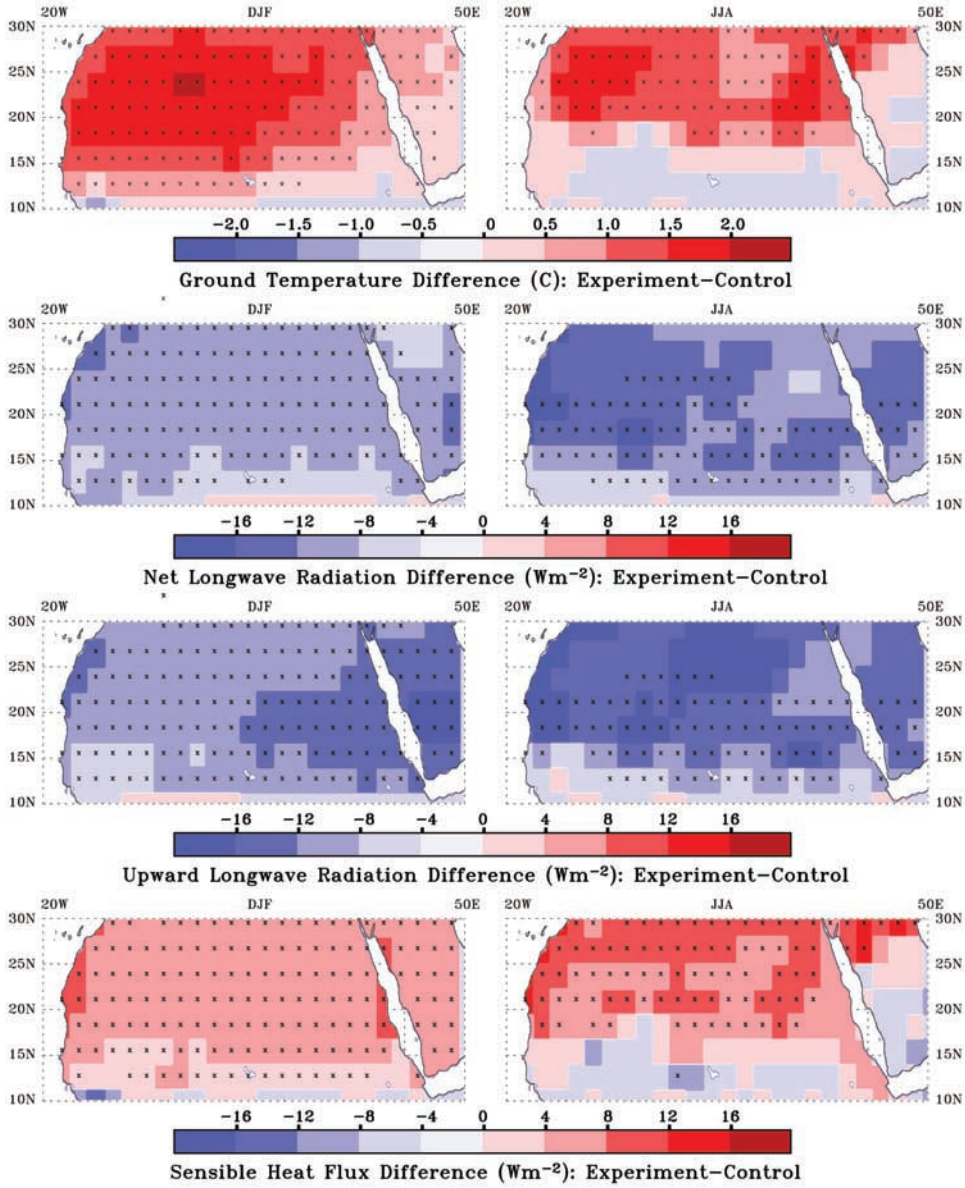

Figure 7. Spatial distributions of differences in ground temperature, net longwave radiation, upward longwave radiation, and sensible heat flux between the control run and the experiment with the soil emissivity of 0.84 averaged from 1979 to 1998 in winter (DJF) and summer (JJA). The symbol "x" denotes grid cells with a significant difference at the 5% level.

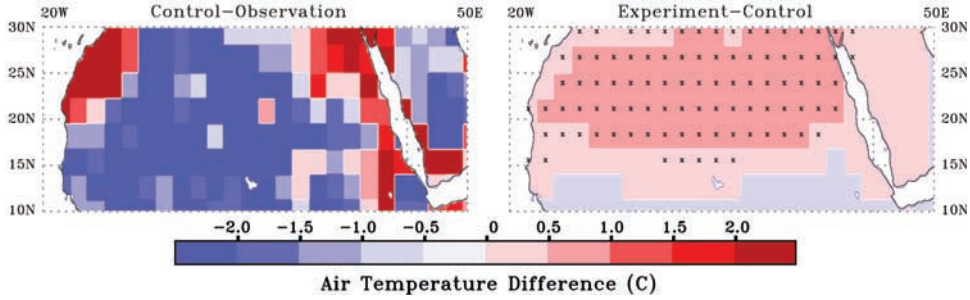

Figure 8. Spatial patterns of differences in annual mean surface air temperature between observations and model simulations from the control run and the experiment with the soil emissivity of 0.88 averaged from 1979 to 1998: control-observation (left panel) and experiment-control (right panel). The symbol "x" denotes grid cells with a significant difference at the 5% level.

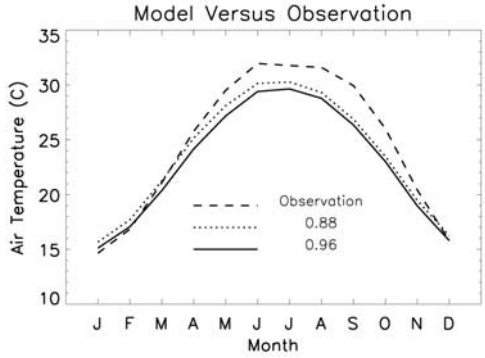

Figure 9. Seasonal variations in surface air temperature between observations and model simulations from the control run and the experiment with the soil emissivity of 0.88 averaged over 17°N–30°N, 0°E–30°E from 1979 to 1998.

a smaller $\Delta T_g/\Delta\varepsilon_g$. $\bar{L}$ and $L\uparrow$ have an opposite seasonal cycle to that of temperature, and H has the largest change in spring and the smallest change in fall. The seasonal difference between temperature and other variables may be also related to variations and feedbacks of T_g and $L\downarrow$ in equation (6) and changes of other terms in equation (1) as previously discussed. Figure 6 shows the diurnal variations in UT of the estimated slopes for T_a, $\bar{L}$, $L\uparrow$, and H. All variables show a significant day-night difference. Air temperature increases almost twice as much during nighttime (maximizes around 5 am) as during daytime (minimizes around 3 pm) while the other variables show an opposite diurnal cycle. The day-night difference can be similarly explained by equation (6) as the summer-winter difference. Both are accounted for by the greater cancellation by sensible heat changes for an unstable surface layer. Except a few cases, the majority of the seasonal and diurnal slopes are statistically significant at the 5% level.

[19] Figure 7 shows spatial differences in T_g, $\bar{L}$, $L\uparrow$, and H between the control run and the experiment with the soil emissivity of 0.84. Evidently, ground temperature shows a larger increase in magnitude and spatial range in winter than in summer, while the other variables show an opposite seasonal difference, consistent with the previous discussion. Over the vegetated grid cells (Figure 3), the differences are generally small for all four variables, and a small decrease in temperature and sensible heat flux is observed. A t test is performed to test whether the difference at each grid cell is statistically significant. Our results indicate that the majority of the model grid cells show a significant difference at the 5% level.

3.3. Comparison With Observed Surface Air Temperature

[20] Observed monthly terrestrial air temperature (C. J. Willmott and K. Matsuura, Terrestrial air temperature and precipitation: Monthly and annual time series (1950–1999), version 1.02, available at http://climate.geog.udel.edu/~climate, 2001) from January 1979 to December 1998 is compared with our model simulations from both the control run and the experiment with the soil emissivity of 0.88. The latter is chosen because it is the dominant value for bare soil from satellite observations as discussed in section 2.1. A total number of 7280 Global Historical Climatology Network stations was used to generate the temperature data set. Figure 8 shows spatial patterns of differences in annual mean air temperature between model simulations and observations. The CLM2 shows a cold bias larger than 2 degrees over a broad region in the central Sahara (left panel), consistent with *Bonan et al.* [2002]. When the emissivity of 0.88 was used, on average, the cold bias could be partially reduced by more than 0.5°C over most regions (right panel). Figure 9 shows seasonal variations of air temperature averaged from 1979 to 1998 between model simulations and observations. The use of emissivity of 0.88 helps to reduce the cold bias present for most months. The remaining differences are presumably a consequence of some difficulties in either the model or the observational data.

4. Conclusions and Discussion

[21] This paper analyzes the sensitivity of simulated climate and energy balance to changes in soil emissivity over Northern Africa and the Arabian Peninsula, and considers how this information may be used to improve emissivity parameterizations in climate models. Five 20-year sensitivity experiments based on satellite observations are performed using the recently developed Community Land Model (CLM2). Relationships between changes in soil emissivity and changes in simulated climate and energy balance variables are analyzed.

[22] Satellite derived emissivity (8–13.5 μm) for bare soil ranges from 0.83 to 0.96 and more than half of pixels over our study region have emissivity values less than 0.90 while the CLM2 uses a constant value of 0.96, suggesting the model soil emissivity is too high over this region. Our sensitivity tests indicate that this bias could produce significant errors in model simulated ground and air temperature, net and upward longwave radiation, and sensible heat flux. There is a linear relationship between changes in emissivity and changes in these variables. Statistical results indicate that, on average for the study region, a decrease of soil emissivity by 0.1 will increase ground and air temperature by about 1.1°C and 0.8°C and decrease net and upward longwave radiation by about 6.6 Wm^{-2} (less emission) and 8.1 Wm^{-2}, respectively, at the ground surface. The decreased longwave emission is mainly released to the atmosphere through an increase of the sensible heat flux of about 5.9 Wm^{-2}. These relations vary seasonally and diurnally. The temperature increases are slightly higher in winter than in summer and twice as large during nighttime as during daytime, while the other variables show more change in summer/daytime than in winter/nighttime. Our experimental results are consistent with our theoretical energy balance analyses. If a more realistic emissivity value were used, the model cold bias over the Sahara in comparison with land surface air temperature observations would be partially reduced.

[23] These results indicate that the simple representations of the land surface emissivity in current climate models, especially for bare soil, need improvement based on satellite and in situ observations. The land surface emissivity varies with surface type, vegetation amount, and soil moisture, and shows considerable spatial and temporal variations in sat-

ellite observations, especially over the Sahara desert where the largest variability is observed [*Ogawa et al.*, 2002; 2003; *Jin and Liang*, 2004; *Zhou et al.*, 2003a].

[24] **Acknowledgments.** This work was funded by the NASA EOS/IDS Program (NAG5-8880).

References

Bonan, G. B., A land surface model (LSM version 1.0) for ecological, hydrological, and atmospheric studies: Technical descriptions and user guide, *NCAR Tech. Note, NCAR/TN-417+STR*, 150 pp., Natl. Cent. Atmos. Res., Boulder, Colo., 1996.

Bonan, G. B., K. W. Oleson, M. Vertenstein, S. Levis, X. Zeng, Y. Dai, R. E. Dickinson, and Z. Yang, The land surface climatology of the NCAR community land model coupled to the NCAR Community Climate Model, *J. Clim.*, *15*, 3123–3149, 2002.

Dai, Y., et al., The Common Land Model (CLM) version 1.0, *Bull. Am. Meter. Soc.*, *84*(8), 1013–1023, 2003.

Dickinson, R. E., A. Henderson-Seller, and P. J. Kennedy, Biosphere-Atmosphere Transfer Scheme (BATS) Version le as coupled to the NCAR Community Model, *NCAR Tech. Note, NCAR/TN-387+STR*, 72 pp., Natl. Cent. Atmos. Res., Boulder, CO, 1993.

Friedl, M. A., et al., Global land cover from MODIS: Algorithms and early results, *Remote Sens. Environ.*, *83*, 287–302, 2002.

Jin, M., and S. Liang, Improving land surface emissivity parameter of land surface model in GCM, *J. Clim.*, in press, 2004.

Kinter, J. L., III, J. Shukla, L. Marx, and E. K. Schneider, A simulation of the winter and summer circulations with the NMC global spectral model, *J. Atmos. Sci.*, *45*, 2486–2522, 1988.

Ogawa, K., T. Schmugge, and A. French, Estimation of broadband land surface emissivity from multi-spectral thermal infrared remote sensing, *Agronomie*, *22*(6), 695–696, 2002.

Ogawa, K., T. Schmugge, and F. Jacob, Estimation of land surface window (8–12 μm) emissivity from multispectral thermal infrared remote sensing: A case study in a part of Sahara Desert, *Geophys. Res. Lett.*, *30*(2), 1067, doi:10.1029/2003GL016354, 2003.

Ogawa, K., T. J. Schmugge, F. Jacob, and A. French, Mapping surface broadband emissivities of Sahara Desert using ASTER and MODIS data, *Earth Interact.*, in press, 2004.

Oleson, K. W., G. B. Bonan, C. B. Schaaf, F. Gao, Y. Jin, and A. Strahler, Assessment of global climate model land surface albedo using MODIS data, *Geophy. Res. Lett.*, *30*(8), doi:10.1029/2002GL016749, 2003.

NMC Development Division, Documentation of the research version of the NMC Medium-Range Forecasting model, 504 pp, NMC Develop. Div., Natl. Meteorol. Cent., Camp Springs, MD, 1988.

Prabhakara, C., and G. Dalu, Remote sensing of the surface emissivity at 9 μm over the Globe, *J. Geophys. Res.*, *81*(21), 3719–3724, 1976.

Salisbury, J. W., and D. M. D'Aria, Emissivity of terrestrial materials in the 8–14 μm atmospheric window, *Remote Sens. Environ.*, *42*, 83–106, 1992.

Sellers, P. J., et al., Modeling the exchanges of energy, water and carbon between the continents and the atmosphere, *Science*, *275*, 502–509, 1997.

Tian, Y., Y. Wang, Y. Zhang, Y. Knyazikhin, J. Bogaert, and R. B. Myneni, Radiative transfer based scaling of LAI/FPAR retrievals from reflectance data of different resolutions, *Remote Sens. Environ.*, *84*, 143–159, 2002.

Wilber, A. C., D. P. Kratz, and S. K. Gupta, Surface emissivity maps for use in satellite retrievals of longwave radiation, *NASA/TP-1999-209362*, pp. 30, NASA, Greenbelt, Md., 1999.

Zeng, Q. C., X. H. Zhang, X. Z. Liang, C. G. Yuan, and S. F. Chen, Documentation of IAP two-level atmospheric general circulation model, *DOE/ER/60314-HI*, 383 pp., U. S. Dept. of Energy, Washington, D. C., 1989.

Zeng, X., M. Shaikh, Y. Dai, R. E. Dickinson, and R. B. Myneni, Coupling of the common land model to the NCAR community climate model, *J. Clim.*, *14*, 1832–1854, 2002.

Zhou, L., R. E. Dickinson, K. Ogawa, Y. Tian, M. Jin, T. Schmugge, and E. Tsvetsinskaya, Relations between albedos and emissivities from MODIS and ASTER data over North African desert, *Geophy. Res. Lett*, *30*(20), 2026, doi:10.1029/2003GL018069, 2003a.

Zhou, L., et al., Comparison of seasonal and spatial variations of albedos from MODIS and Common Land Model, *J. Geophys. Res.*, *108*(D15), 4488, doi:10.1029/2002JD003326, 2003b.

R. E. Dickinson, Y. Tian, H. Yu, and L. Zhou, School of Earth and Atmospheric Sciences, Georgia Institute of Technology, Atlanta, GA 30332, USA. (lmzhou@eas.gatech.edu)

M. Jin, Meteorology Department, University of Maryland, College Park, MD 20742, USA.

K. Ogawa and T. Schmugge, USDA/ARS Hydrology and Remote Sensing Lab, Beltsville, MD 20705, USA.